GFZ
Helmholtz-Zentrum
POTSDAM

Originally published as:

Weller, O., Lange, D., Tilmann, F., Natawidjaja, D. H., Rietbrock, A., Collings, R. E., Gregory, L. (2012): The structure of the Sumatran Fault revealed by local seismicity. - Geophysical Research Letters, 39, L01306

DOI: 10.1029/2011GL050440

The structure of the Sumatran Fault revealed by local seismicity

O. Weller,[1,2] D. Lange,[2,3] F. Tilmann,[2,3] D. Natawidjaja,[4] A. Rietbrock,[5] R. Collings,[5] and L. Gregory[1]

Received 29 November 2011; accepted 4 December 2011; published 11 January 2012.

[1] The combination of the Sunda megathrust and the (strike-slip) Sumatran Fault (SF) represents a type example of slip-partitioning. However, superimposed on the SF are geometrical irregularities that disrupt the local strain field. The largest such feature is in central Sumatra where the SF splits into two fault strands up to 35 km apart. A dense local network was installed along a 350 km section around this bifurcation, registering 1016 crustal events between April 2008 and February 2009. 528 of these events, with magnitudes between 1.1 and 6.0, were located using the double-difference relative location method. These relative hypocentre locations reveal several new features about the crustal structure of the SF. Northwest and southeast of the bifurcation, where the SF has only one fault strand, seismicity is strongly focused below the surface trace, indicating a vertical fault that is seismogenic to ~15 km depth. By contrast intense seismicity is observed within the bifurcation, displaying streaks in plan and cross-section that indicate a complex system of faults bisecting the bifurcation. In combination with analysis of topography and focal mechanisms, we propose that the bifurcation is a strike-slip duplex system with complex faulting between the two main fault branches. **Citation:** Weller, O., D. Lange, F. Tilmann, D. Natawidjaja, A. Rietbrock, R. Collings, and L. Gregory (2012), The structure of the Sumatran Fault revealed by local seismicity, *Geophys. Res. Lett.*, *39*, L01306, doi:10.1029/2011GL050440.

1. Introduction

[2] The Sumatran Fault (SF) is a 1900 km long dextral fault that runs the length of Sumatra in Indonesia (Figure 1). In the Sumatra region the Australian and Eurasian plates converge along the Sunda megathrust [e.g., *McCaffrey*, 2009]. Relative motion is perpendicular to the Sunda trench offshore of Java, and convergence is accommodated by motion on the megathrust. As the trench curves around Sumatra, relative motion becomes oblique up to ~40°. Slip-vectors on the megathrust are also observed to rotate, broadly maintaining trench-perpendicular motion [*McCaffrey*, 1991]. This leaves a trench-parallel shear component, which is accommodated mostly by the SF. Several fault systems dissecting the forearc (e.g., the Mentawai and Batee faults) have also been proposed to accommodate some strike-slip motion [*Diament et al.*, 1992; *McCaffrey et al.*, 2000; *Collings et al.*, 2012], but it is not clear whether these faults are currently active in a strike-slip sense (rather than as thrusts [e.g., *Singh et al.*, 2010]). The broad division of trench-normal strain on the megathrust and trench-parallel shear strain on the SF is known as slip-partitioning, and the Sumatra region has long been cited as a classic example of this behaviour [*Fitch*, 1972]. The slip rate varies along the SF but recent GPS data suggest the slip rate is uniform across central Sumatra at 21 ± 5 mm/a [*Genrich et al.*, 2000]. More than 42 events with M ≥ 5 have occurred during the last four decades [*Petersen et al.*, 2004] and the SF is capable of producing major earthquakes, such as the magnitude 7.7 earthquake in 1892 that produced dislocations of at least 2 m [*Reid*, 1913].

[3] *Sieh and Natawidjaja* [2000] studied the geomorphology of the SF in detail and found that it is highly segmented, with second order geometrical irregularities splitting the fault into 19 major segments. The largest irregularity is at the equator where the fault splits into two sub-parallel strands up to 35 km apart; a structure coined the 'equatorial bifurcation' [*Sieh and Natawidjaja*, 2000]. However, the region is tropical and the SF coincides spatially with the magmatic arc so some parts of the SF may be disguised by erosion and volcanism, respectively. A paleoseismological study in the region found few seismic horizons relative to historical records [*Bellier et al.*, 1997], and little is known about the crustal structure of the SF and its relation to the magmatic arc.

[4] The aim of this study is to illuminate the sub-surface structure of the SF using hypocentre locations of crustal seismicity registered with a dense local network. This approach is only appropriate if the error bars associated with the calculated locations of seismicity can be minimised relative to the scale of fault structures. In this study we take advantage of a dense local network to apply the double-difference relative earthquake relocation method [*Waldhauser and Ellsworth*, 2000] in order to provide a detailed description of the internal structure of the bifurcation, identifying it as a strike-slip duplex.

2. Data and Methods

[5] Seismic data were collected by installation of a local network of 54 land-stations (large white triangles, Figure 1) from April 2008 to February 2009 [*Lange et al.*, 2010]. Azimuthal coverage was improved by incorporating data from eight permanent stations from the Indonesian Meteorological and Geophysical Agency and stations GSI and BKNI from the German GEOFON network. Additionally, stronger events were located using additional data from temporary arrays to the north [*Stankiewicz et al.*, 2010] and south [*Collings et al.*, 2012]. This study focuses on the

[1]Department of Earth Sciences, University of Oxford, Oxford, UK.
[2]Formerly at Bullard Laboratories, Department of Earth Sciences, University of Cambridge, Cambridge, UK.
[3]Helmholtz Center Potsdam, GFZ German Research Centre for Geosciences, Potsdam, Germany.
[4]LabEarth, Indonesian Institute of Sciences, Bandung, Indonesia.
[5]Earth and Ocean Sciences, University of Liverpool, Liverpool, UK.

Copyright 2012 by the American Geophysical Union.
0094-8276/12/2011GL050440

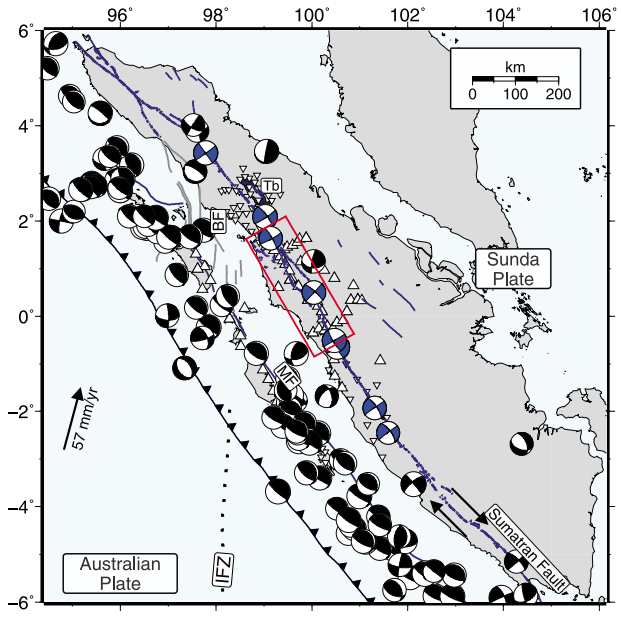

Figure 1. Location map showing the tectonic setting of the Sumatran margin. Focal mechanisms (Global CMT catalogue, 1976–2010) show mainly thrust events with strikes parallel to the trench. Shallow events along the SF (<40 km shown in blue) show exclusively dextral focal mechanisms. The continuous blue line on the land surface indicates the Sumatran fault (SF) [*Sieh and Natawidjaja*, 2000]. The black arrow shows the convergence rate from *Natawidjaja et al.* [2006]. The locations of seismic stations used in this study are indicated by triangles. Stations shown with inverted white triangles were only included for the stronger events and for events along the SF just to the northwest of our network. More information about the seismic network(s) is given by *Lange et al.* [2010]. The red box is the area shown in Figure 2. Abbreviations: Tb: Lake Toba, MF: Mentawai fault, BF: Batee fault, IFZ: Investigator Fracture Zone.

crustal seismicity within the boxed region of Figure 1; the forearc and intermediate-depth events located by these networks are discussed by *Lange et al.* [2010] and *Collings et al.* [2012].

[6] 1016 shallow events along the SF were recorded and over 21,000 corresponding P- and S-phase arrivals were manually picked [*Lange et al.*, 2010]. The largest earthquake was the M_w 6.0 event on 19 May 2008 at the northern end of the bifurcation (red circle, Figure 2), with a dense aftershock sequence up to M_w 5.3. The events were initially inverted in VELEST [*Kissling et al.*, 1994] for a minimum 1D velocity model of the continental crust and hypocentre locations. We only included events with more than 8 onset times, containing at least 4 S-wave observations, and a GAP (= the largest azimuthal range with no observations) smaller than 180°. This reduced the number to 428 well-constrained events with 6,565 P- and 4,440 S-wave travel time observations. We first inverted a minimum RMS 1-D P-wave velocity model using a constant v_p/v_s ratio of 1.77 derived from Wadati diagrams. The minimum 1-D S-wave velocity model was then determined by an additional series of inversions with different initial v_p/v_s ratios following *Husen et al.* [1999] (Figure S1 in the auxiliary material).[1] The model is well resolved between depths of 5 and 50 km.

[7] We use the double-difference earthquake location algorithm of *Waldhauser and Ellsworth* [2000] to further refine the locations. This algorithm is only appropriate for regions of dense seismicity and station coverage. Essentially, the hypocentral separation between two earthquakes must be small compared to the event-station distance and velocity heterogeneity scale length so that the ray paths for two events observed at a common station will be similar along almost the entire ray path. The fundamental data used in the algorithm (hypoDD) are the 'double-differences': the difference between the observed and predicted phase arrival time for pairs of earthquake observed at the same station. 101,274 travel time differences from 995 events were obtained from manual picks of phases, and 16,723 from cross-correlation waveform analysis. The algorithm relates the double-difference to changes in the vector connecting their (relative) hypocenters. Minimising this residual achieves high-resolution relative hypocenter locations because absolute errors are of common origin, except where ray paths differ near source. By linking together chains of events that qualify as neighbours, high-resolution relative hypocenter locations over large distances are obtained. We used the conjugate gradients method (LSQR) implemented in hypodDD [*Waldhauser and Ellsworth*, 2000] to solve the large inverse problem posed by the double-difference algorithm. The neighbour threshold used was 10 links, with stations no more than 80 km from the event pairs. 528 events met this threshold and produced stable relative hypocentral coordinates. Given that the errors are estimated poorly by LSQR the robustness of the relocation was tested through jackknife tests. We randomly ignored between 15 and 30% of the observations (picks) for certain (stronger) events and introduced these reduced subsets into the location routine from VELEST. Using these updated (absolute) hypocentre locations we relocated the events with hypoDD. The jackknife tests resulted in formal errors for 482 events; the location errors are typically smaller than 500 m for the horizontal hypocentral coordinates and 1250 m for the depth. Due to the relocation with VELEST and the reduced number of picks we regard the result of the jackknife tests as a conservative measure of the formal error. Since the elongation of the resulting hypocentres is (for most of the events) smaller than the length of the streaks, the linear elongation of the clusters is resolved (e.g., section A of Figure S2).

[8] Additionally, we calculated fault plane solutions from P-wave first polarities for events with $M_l \geq 3$, GAP $\leq 180°$ and more than 15 polarity readings using FPFIT [*Reasenberg and Oppenheimer*, 1985]. 10 events produced unique solutions and are shown in Figure 2.

3. Results

[9] The final relative hypocenter locations are plotted in Figure 2, with blue circles denoting the best-constrained events. Northwest of the bifurcation seismicity is localised to the surface trace of the SF and mostly comprises the magnitude M_w 6.0 event (red circle, focal mechanism 3) and its aftershocks, which stop at Sibualbuali volcano. The

[1] Auxiliary materials are available in the HTML. doi:10.1029/2011GL050440.

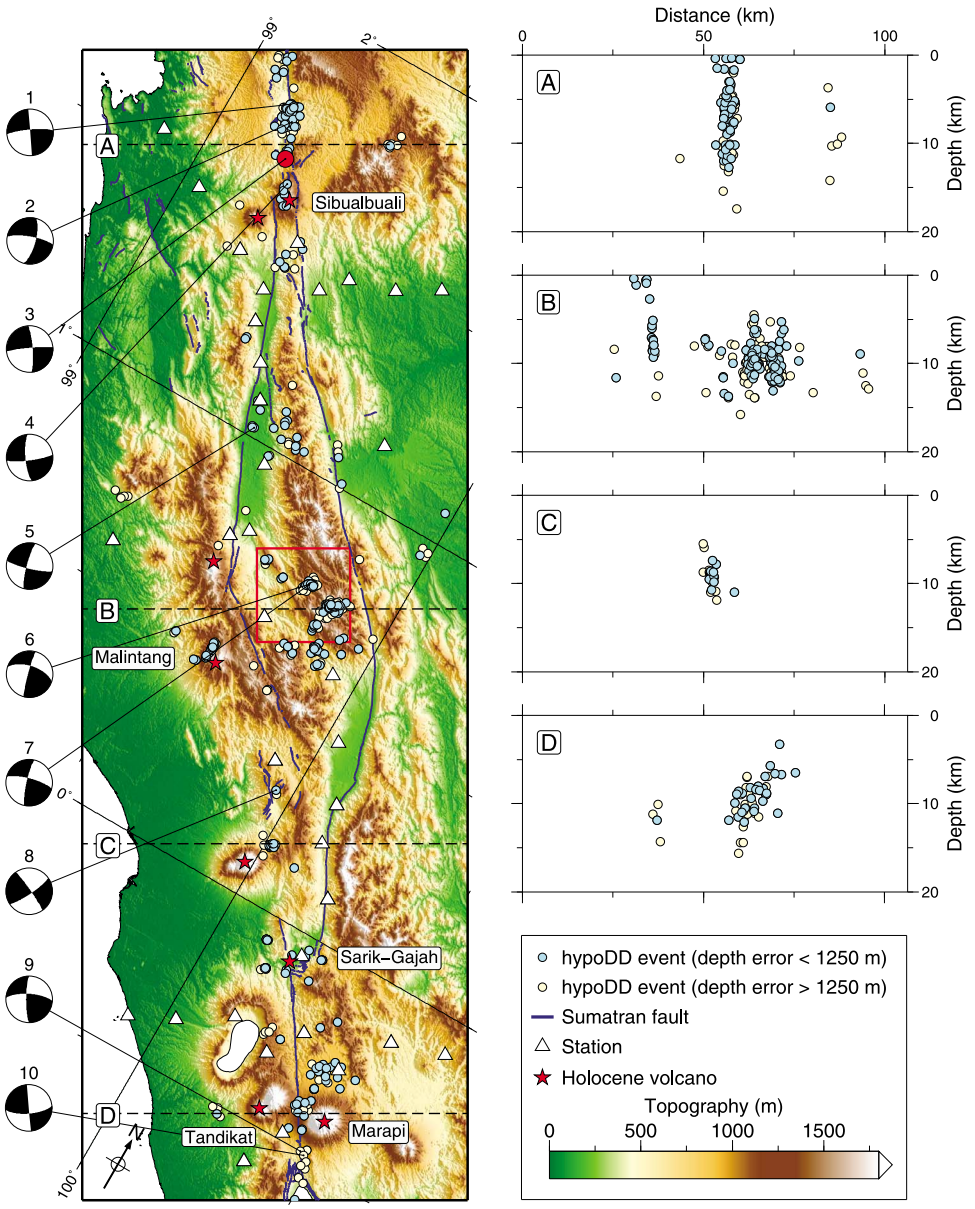

Figure 2. Overview of seismicity in the study area. The plan view is an oblique Mercator projection. Each circle is an event detected by the local seismic network (white triangles) and located using the hypoDD method outlined in the text. The light blue events are the best constrained and have a depth error smaller than 1250 m. The red circle highlights the largest earthquake during deployment: a M_w 6.0 event on 19 May 2008. The red box is the area shown in Figure 3. The cross-sections have 20 km swath ranges and 2:1 vertical exaggeration. Focal mechanisms for a sub-set of the 10 highest quality events are displayed. Volcanoes (Smithsonian Institute) shown with red stars. Topography is Shuttle Radar Topography Mission (90 m resolution) elevation data [*Farr et al.*, 2007].

seismicity on the corresponding cross-section (Figure 2, section A) delineates the SF to be a single vertical fault, with seismic activity down to depths of ~15 km. A previous temporary network [*Masturyono et al.*, 2001] also observed seismicity limited to a single strand in this area. Southeast of the bifurcation a cluster of seismicity leaves the fault trace at 0.4°S between the Marapi and Tandikat volcanoes. This marks the onset of heterogeneous strain on approach to the bifurcation, with splay faulting seen in the surface trace, slightly more variable focal mechanism strikes, and seismicity no longer aligned with the major fault traces. Further south the seismicity is once again aligned narrowly with the fault trace, again showing a seismogenic thickness of ~15 km.

[10] Within the bifurcation (between 0.1°S and 1.5°N), the geomorphology is consistent with dextral faulting across step-overs, with a ridge at each contractional left-step and a basin at each dilatational right-step (Figure 2). This matches the broad fault trace from *Sieh and Natawidjaja* [2000]. However, the seismicity distribution reveals a more complex structure, as large amounts of seismicity are located away from the known fault trace within the middle of the bifurcation. The seismicity displays streaks in plan view that form linear dipping structures in section (e.g., Figure 2,

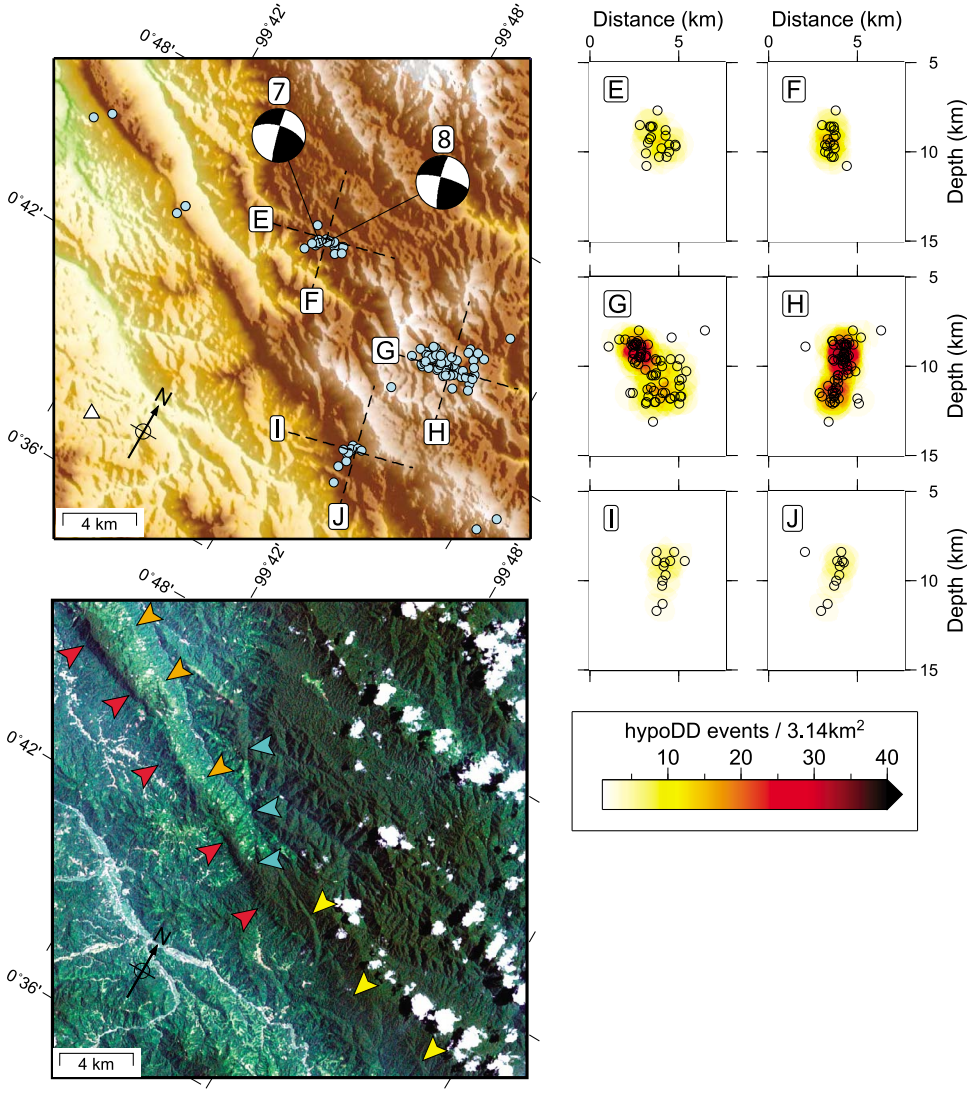

Figure 3. Close-up of the equatorial bifurcation. The key for the plan view (top left) is as for Figure 2. Topography is ASTER G-DEM (30 m resolution). The events are shown as empty circles in cross-section (right). The cross-sections have 6 km swath ranges, no vertical exaggeration, and are orientated with respect to their labels. They are underlain by a density plot that counts events within a 1 km radius. The region is also shown as a Landsat satellite image (bottom left, 30 m resolution) with bands 3, 2, 1 in RGB. Coloured arrows point to four different lineations that could be geomorphic expressions of active faults (see text for details), but are not necessarily linked to the seismic clusters.

section B). Prominent linear ridges are also seen in the topography in this region, bisecting the bifurcation parallel to the contractional limbs of the SF.

[11] This region of the bifurcation is examined in more detail in Figure 3, using higher resolution topographic data and Landsat satellite imagery to analyse the geomorphology, reduced swath ranges to distinguish clusters, an underlay to the cross-sections to show event density and equal-scale cross-sections orientated parallel to nodal planes from nearby focal mechanisms to gauge fault dip and orientation. This reveals that the majority of seismicity is concentrated into three clusters (E/F, G/H and I/J), demonstrating that strain is not diffusely distributed, but localised to individual faults within the bifurcation. Furthermore, the clusters have variable strike and dip, indicating a departure from the homogeneous dextral strain seen outside the bifurcation. Elongation of the cluster E/F along cross-section E in the WSW direction, compared with the vertical distribution in cross-section F, indicates a WSW oriented fault. Given the polarity of focal mechanisms 7 and 8, this suggests that the fault is sinistral. This conclusion is also supported by *Rock et al.* [1983], who noted field evidence of sinistral movement in this region. A similar relationship also holds for the G/H cluster, with elongation to the WSW, though this fault also shows in section H a small dip component towards the centre of the bifurcation. With only 12 events, cluster I/J appears to have a nearly linear form with no clearly defined fault plane.

[12] Active faults can be recognised as lineations in Landsat satellite imagery in the vicinity of these seismic clusters, as shown in Figure 3 (bottom left). In the image, arrows of different colour indicate the geomorphic expression of potential fault strands. The red and orange arrows point to two linear changes in slope along the base of a

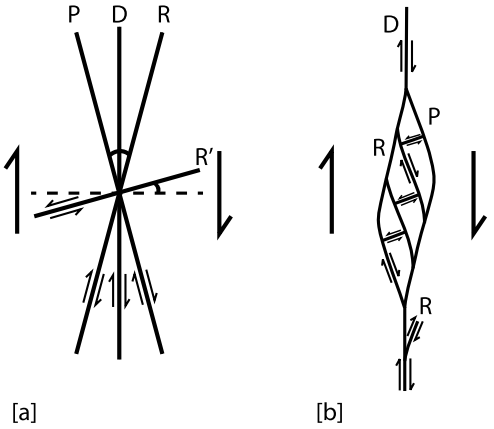

Figure 4. (a) Ideal fault orientations in a dextral strike-slip system, as described by *Woodcock and Fischer* [1986]. R and R′ are conjugate Riedel shears that form at low displacement (note the sinistral characteristics of the R′ shears); P and D are shears that form at higher displacements. (b) One example of how duplex geometries may form on a straight segment by various interactions amongst these shears.

prominent fault-propagated ridge. The lineations are especially apparent because of the contrast in drainage steepness on either side of the fault, with much greater incision on the up-thrown side of the fault, indicating some dip-slip motion. The blue and yellow arrows indicate a break in slope typical of active oblique-slip faults, where horizontal motion of a sloping surface leads to an apparent reversal or step in the slope along the trace of the fault. While the lineations are not necessarily linked directly to the discrete seismicity observed in this study, the geomorphic evidence of faulting does corroborate the notion that additional faults bisect the bifurcation. The faults bounding the bifurcation also have a very clear geomorphic expression, with multiple along-strike offsets of major drainages by up to 5 km [*Sieh and Natawidjaja,* 2000].

[13] Several small clusters of seismicity lie off the SF and out of the bifurcation. The largest off-fault cluster, at 99.6°E/0.5°N, forms a linear streak beneath the stratovolcano Malintang (Figure 2, section B), with events well located between 0 and 10 km depth. Malintang has had no known historical eruptions, but these earthquakes may reflect fluid movement, potentially indicating an elevated risk of eruption. However there has been no reported activity since the deployment in 2008, and recent InSAR studies have not found any coherent signals of deformation in the region [*Chaussard et al.*, 2009]. On the south-eastern side of the bifurcation sparse seismicity is spatially associated with the andesitic-basaltic cone Sarik and the andesitic-dacitic cone Gajah. All other Holocene volcanoes in the area did not have seismicity in close vicinity during the deployment. Some small off-fault clusters are not associated with volcanoes (e.g., near 1°N, 100°E), but these are generally less well constrained as they are on the periphery of the network.

4. Discussion

[14] Well-constrained seismicity is a useful complement to geomorphology studies because it reveals faults with no (or disguised) surface expression. While the technique will never capture the full picture, because only some parts of a fault system are illuminated by seismicity during any one deployment, it serves to focus attention on new areas. In this study, the intense seismicity observed within the bifurcation away from the surface fault trace suggests additional complexity. The seismicity is not diffuse, but forms dense linear streaks that suggest additional active faults splay from the SF and bisect the bifurcation. This is corroborated by lineations in the topography that suggest Quaternary faulting in the region (Figure 3).

[15] The overall geometry is consistent with a structure called a 'strike-slip duplex' (Figure 4), which is described as a zone of steep imbricate faults that are typically bounded by two continuous major fault zones, between which smaller en-echelon faults define the duplex structure and may converge downwards to form a flower structure in cross-section [*Woodcock and Fischer*, 1986; *Cunningham and Mann*, 2007]. By analogy, the current fault trace of the bifurcation maps the bounding faults, and the internal seismicity represents partial illumination of en-echelon faults and flower structures. This could explain the prominent topography and the variable dip of the seismic streaks in the central part of the bifurcation.

[16] Strike-slip duplexes can form in a variety of settings, such as at bends or offsets in strike-slip systems, and subsequent shunting of the duplex can make inferring formation conditions difficult. However, we consider that formation on a straight segment from linking together conjugate and en-echelon Riedel shears [*Woodcock and Fischer*, 1986] to be the most likely scenario. Figure 4a shows the ideal orientation of these shears, and it is notable that in a dextral setting, sinistral shears (R′) should be orientated at a high angle to the bounding faults, as proposed for focal mechanisms 7 and 8. This mechanism also makes splay faults common on approach to a duplex from un-linked R shears, as proposed for the cluster of seismicity trending north of Marapi. These shears can interact in different ways to produce duplex geometries, with Figure 4b showing one example that is similar to the orientation of faults seen in this study. In an overall dextral setting, the current orientation of the sinistral faults is consistent with bookshelf vertical-axis rotation tectonics [e.g., *England and Molnar*, 1990].

[17] *McClay and Bonora* [2000] use sandbox modelling to analyse the geometric and kinematic development of duplex structures. Their models suggest that real-world duplexes are even more complicated than the schematic shown in Figure 4b, with multiple root structures and composite deformation patterns within the duplex. The overall geometry of a duplex is also unstable with time and continued slip will require the structure to widen. Therefore, duplexes are regions of significant internal deformation, consistent with our observation of intense (micro) seismicity largely between the bounding faults. Conversely, it is likely that the major release of strain occurs on the less segmented, single-strand regions of the SF, as suggested by the longer-term CMT record in Figure 1. This duality of behaviour makes the bifurcation ideal for local seismicity studies, because density of seismicity is necessary for both application of hypoDD and for illumination of faults. A longer term, more focused array (coupled with accurate relocation algorithms) could further reveal the duplex

structure, as this study shows that the deformation is contained on discrete faults within the bifurcation.

[18] The suggested seismogenic thickness of 15 km for the SF is less than the 25 km reported using local seismicity from the 1994, M_w 6.8 Liwa earthquake in Southern Sumatra [*Widiwijayanti et al.*, 1996], but similar to maximal reported earthquake depths of continental seismicity along other strike-slip faults along volcanic arcs, such as the Liquiñe-Ofqui fault Zone in Southern Chile [*Lange et al.*, 2008].

5. Conclusions

[19] Using double-differences, high precision relative locations have been determined for 528 events along the central part of the SF. Analysis of the event distribution and topography indicates that strain is highly localized to the SF away from the bifurcation, with maximal depths of 15 km, but within the bifurcation (between 0.1°S and 1.5°N), most seismicity is found off the two main bounding fault traces identified by *Sieh and Natawidjaja* [2000]. Instead, seismicity is found within the bifurcation, where there also appears to be a number of faults with geomorphic expression. Based on the overall geometry, we suggest that the equatorial bifurcation is a strike-slip duplex with complex structure between the main fault branches. Seismicity during the deployment is also found beneath the stratovolcanoes Malintang and Sibualbuali and the volcanic cones of Sarik-Gajah. All other Holocene volcanoes have no seismicity in their close vicinity during the deployment.

[20] **Acknowledgments.** We thank the SeisUK facility in Leicester for the loan of the instruments and the continuing logistic support of this project. GFZ instruments were provided by the GIPP, and we thank C. Haberland for making these available. We acknowledge the great support of the colleagues at Geotek-LIPI for this project. EOS (Earth Observatory of Singapore) supported logistical costs of deployment on Mentawai and Batu islands. We thank the Indonesian BMKG and German GEOFON for providing data from their permanent networks, and all field crews for their excellent work. We thank Nano Seeber for a stimulating review and an anonymous reviewer for further constructive comments. ASTER data are distributed by the Land Processes Distributed Active Archive Center (LP DAAC). The project is funded by NERC (NE/D00359/1). Cambridge Dep. of Earth Sci. publication esc.2321.

References

Bellier, O., M. Sébrier, S. Pramumijoyo, T. Beaudouin, H. Harjono, I. Bahar, and O. Forni (1997), Paleoseismicity and seismic hazard along the Great Sumatran Fault (Indonesia), *J. Geodyn.*, *24*(1–4), 169–183, doi:10.1016/S0264-3707(96)00051-8.

Chaussard, E., S. Hong, and E. Amelung (2009), Monitoring the Sumatra volcanic arc with InSAR, *Eos Trans AGU*, *90*(52), Fall Meet. Suppl., Abstract G41A-0703.

Collings, R., D. Lange, A. Rietbrock, F. Tilmann, D. H. Natawidjaja, B. W. Suwargadi, M. Miller, and J. Saul (2012), Structure and seismogenic properties of the Mentawai segment of the Sumatra subduction zone revealed by local earthquake travel-time tomography, *J. Geophys. Res.*, doi:10.1029/2011JB008469, in press.

Cunningham, W. D., and P. Mann (2007), Tectonics of strike-slip restraining and releasing bends, *Geol. Soc. Spec. Publ.*, *290*(1), 1–12, doi:10.1144/SP290.1.

Diament, M., H. Harjono, K. Karta, C. Deplus, D. Dahrin, M. T. Zen Jr., M. Gérard, O. Lassal, A. Martin, and J. Malod (1992), Mentawi fault zone off Sumatra: A new key to the geodynamics of western Sumatra, *Geology*, *20*(3), 259–262, doi:10.1130/0091-7613(1992)020<0259:MFZOSA>2.3.CO;2.

England, P., and P. Molnar (1990), Right-lateral shear and rotation as the explanation for strike-slip faulting in eastern Tibet, *Nature*, *344*, 140–142, doi:10.1038/344140a0.

Farr, T. G., et al. (2007), The Shuttle Radar Topography Mission, *Rev. Geophys.*, *45*, RG2004, doi:10.1029/2005RG000183.

Fitch, T. J. (1972), Plate convergence, transcurrent faults, and internal deformation adjacent to Southeast Asia and the western Pacific, *J. Geophys. Res.*, *77*(23), 4432–4460, doi:10.1029/JB077i023p04432.

Genrich, J. F., Y. Bock, R. McCaffrey, L. Prawirodirdjo, C. W. Stevens, S. S. O. Puntodewo, C. Subarya, and S. Wdowinski (2000), Distribution of slip at the northern Sumatran fault system, *J. Geophys. Res.*, *105*(B12), 28,327–28,341, doi:10.1029/2000JB900158.

Husen, S., E. Kissling, E. Flueh, and G. Asch (1999), Accurate hypocentre determination in the seismogenic zone of the subducting Nazca Plate in northern Chile using a combined on-/offshore network, *Geophys. J. Int.*, *138*(3), 687–701, doi:10.1046/j.1365-246x.1999.00893.x.

Kissling, E., W. L. Ellsworth, D. Eberhart-Phillips, and U. Kradolfer (1994), Initial reference models in local earthquake tomography, *J. Geophys. Res.*, *99*(B10), 19,635–19,646, doi:10.1029/93JB03138.

Lange, D., J. Cembrano, A. Rietbrock, C. Haberland, T. Dahm, and K. Bataille (2008), First seismic record for intra-arc strike-slip tectonics along the Liquiñe-Ofqui fault zone at the obliquely convergent plate margin of the southern Andes, *Tectonophysics*, *455*(1–4), 14–24, doi:10.1016/j.tecto.2008.04.014.

Lange, D., F. Tilmann, A. Rietbrock, R. Collings, D. H. Natawidjaja, B. W. Suwargadi, P. Barton, T. Henstock, and T. Ryberg (2010), The fine structure of the subducted Investigator Ridge in western Sumatra as seen by local seismicity, *Earth Planet. Sci. Lett.*, *298*(1–2), 47–56, doi:10.1016/j.epsl.2010.07.020.

Masturyono, R. McCaffrey, D. A. Wark, S. W. Roecker, Fauzi, G. Ibrahim, and Sukhyar (2001), Distribution of magma beneath the Toba caldera complex, north Sumatra, Indonesia, constrained by three-dimensional *P* wave velocities, seismicity, and gravity data, *Geochem. Geophys. Geosyst.*, *2*, 1014, doi:10.1029/2000GC000096.

McCaffrey, R. (1991), Slip vectors and stretching of the Sumatran fore-arc, *Geology*, *19*(9), 881–884, doi:10.1130/0091-7613(1991)019<0881:SVASOT>2.3.CO;2.

McCaffrey, R. (2009), The Tectonic framework of the Sumatran Subduction Zone, *Annu. Rev. Earth Planet. Sci.*, *37*, 345–366, doi:10.1146/annurev.earth.031208.100212.

McCaffrey, R., P. C. Zwick, Y. Bock, L. Prawirodirdjo, J. F. Genrich, C. W. Stevens, S. S. O. Puntodewo, and C. Subarya (2000), Strain partitioning during oblique plate convergence in northern Sumatra: Geodetic and seismologic constraints and numerical modeling, *J. Geophys. Res.*, *105*(B12), 28,363–28,376, doi:10.1029/1999JB900362.

McClay, K., and M. Bonora (2000), Analog models of restraining stepovers in strike-slip fault systems, *AAPG Bull.*, *85*(2), 233–260.

Natawidjaja, D. H., K. Sieh, M. Chlieh, J. Galetzka, B. W. Suwargadi, H. Cheng, R. L. Edwards, J. Avouac, and S. N. Ward (2006), Source parameters of the great Sumatran megathrust earthquakes of 1797 and 1833 inferred from coral microatolls, *J. Geophys. Res.*, *111*, B06403, doi:10.1029/2005JB004025.

Petersen, M. D., J. Dewey, S. Hartzell, C. Mueller, S. Harmsen, A. Frankel, and K. Rukstales (2004), Probabilistic seismic hazard analysis for Sumatra, Indonesia and across the southern Malaysian Peninsula, *Tectonophysics*, *390*(1–4), 141–158, doi:10.1016/j.tecto.2004.03.026.

Reasenberg, P. A., and D. Oppenheimer (1985), Fpfit, fpplot, and fppage: Fortran computer programs for calculating and displaying earthquake fault-plane solutions, *U.S. Geol. Surv. Open File Rep.*, *85–739*, 25.

Reid, H. F. (1913), Sudden Earth-movements in Sumatra in 1892, *Bull. Seismol. Soc. Am.*, *3*, 72–79.

Rock, N. M. S., D. T. Aldiss, J. A. Aspden, M. C. G. Clarke, A. Djunuddin, W. Kartawa Miswar, S. J. Thompson, and R. Whandoyo (1983), *The Geology of the Lubuksikaping Quadrangle, Sumatra*, Geol. Res. and Dev. Cent., Bandung, Indonesia.

Sieh, K., and D. Natawidjaja (2000), Neotectonics of the Sumatran fault, Indonesia, *J. Geophys. Res.*, *105*(B12), 28,295–28,326, doi:10.1029/2000JB900120.

Singh, S. C., N. D. Hananto, A. P. S. Chauhan, H. Permana, M. Denolle, A. Hendriyana, and D. Natawidjaja (2010), Evidence of active back-thrusting at the NE margin of Mentawai Islands, SW Sumatra, *Geophys. J. Int.*, *180*(2), 703–714, doi:10.1111/j.1365-246X.2009.04458.x.

Stankiewicz, J., T. Ryberg, C. Haberland, Fauzi, and D. Natawidjaja (2010), Lake Toba volcano magma chamber imaged by ambient seismic noise tomography, *Geophys. Res. Lett.*, *37*, L17306, doi:10.1029/2010GL044211.

Waldhauser, F., and W. L. Ellsworth (2000), A double-difference location algorithm: Method and application to the northern Hayward Fault, California, *Bull. Seismol. Soc. Am.*, *90*(6), 1353–1368, doi:10.1785/0120000006.

Widiwijayanti, C., J. Déverchère, R. Louat, M. Sébrier, H. Harjono, M. Diament, and D. Hidayat (1996), Aftershock sequence of the 1994, Mw 6.8, Liwa earthquake (Indonesia): Seismic rupture process in a volcanic arc, *Geophys. Res. Lett.*, *23*(21), 3051–3054, doi:10.1029/96GL02048.

Woodcock, N. H., and M. Fischer (1986), Strike-slip duplexes, *J. Struct. Geol.*, *8*(7), 725–735, doi:10.1016/0191-8141(86)90021-0.

R. Collings and A. Rietbrock, Earth and Ocean Sciences, University of Liverpool, 4 Brownlow Street, Liverpool L69 3GP, UK.

L. Gregory and O. Weller, Department of Earth Sciences, University of Oxford, South Parks Road, Oxford OX1 3AN, UK. (owen.weller@earth.ox.ac.uk)

D. Lange and F. Tilmann, Helmholtz Center Potsdam, GFZ German Research Centre for Geosciences, Telegrafenburg, D-14473 Potsdam, Germany.

D. Natawidjaja, LabEarth, Indonesian Institute of Sciences, Jalan Sangkuriang, Bandung 40135, Indonesia.